2022

A Water-Surface Self-Leveling Landing Platform for Small-Scale UAVs

Mbidi Santos

A Water-Surface Self-Leveling Landing Platform for Small-Scale UAVs

_____

A Thesis

Presented to

the Faculty of the Daniel Felix Ritchie School of Engineering and Computer Science

University of Denver

_____

In Partial Fulfillment

of the Requirements for the Degree

Master Of Science

_____

by

Mbidi Santos

November 2022

Advisor: Dr. Matthew Rutherford

Author: Mbidi Santos
Title: A Water-Surface Self-Leveling Landing Platform for Small-Scale UAVs
Advisor: Dr. Matthew Rutherford
Degree Date: November 2022

Abstract

Because many of the most widely used UAVs, such as the Vertical Take-Off and Landing (VTOL), cannot land securely on sloped or fast-changing surfaces, there is a need to design better deployment and landing stations. This document proposes an approach to design a water-surface self-leveling landing platform by implementing the best concept to be used as a safe ground for UAVs to land and deploy on open waters. After conceptualizing multiple design ideas, these options were laid out in a decision matrix with four criteria: degrees of freedom, mechanical complexity, manufacturing, and cost. The chosen concept was the spherical parallel manipulator that provides the most degrees of freedom and design symmetry allowing for an easy manufacturing process and better control precision. This concept proves innovative as it improves the range of motion with lower energy requirements resulting in a device that provides low inertia, high velocity, and precise spherical motion [36]. A spherical parallel manipulator platform was designed in SolidWorks, and then a 3D-printed prototype was assembled and tested. The forward and inverse kinematic of the mechanism were thoroughly analyzed, and tests were performed to verify the ideal inverse kinematic solution.

Acknowledgments

I express my deepest gratitude to Dr. Matt Rutherford, my academic advisor, for his constant supervision and guidance throughout my research. His mentorship and encouragement have been vital in the pursuit of my degree. I also want to thank Dr. Kimon Valavanis for his invaluable advice, support, and guidance during this research. I would like to thank colleagues and ECS staff members. Finally, I would like to thank my family (especially my sister Irina).

Table of Contents

List of Figures

List of Tables

List of Acronyms

2D	Two Dimensional
3D	Three Dimensional
DOF	Degree of Freedom
SPM	Spherical parallel Manipulator
CAD	Computer-Aided Design
DU2SRI	University of Denver Unmanned System Research Institute
IMU	Inertial Measurement Unit
CR	Center of Rotation
UAVs	Unmanned Arial Vehicles
UGV	Unmanned Ground Vehicle
GUI	Graphical User Interface
ASDS	Autonomous Spaceport Drone Ship
RPI	Raspberry-pi
3-RRR	3 Joint Rotation
SPMR	Spherical parallel Manipulator Robot

Chapter 1

1. Introduction

1.1. Background and Motivation

The world relies on Autonomous Unmanned Aerial Vehicles for surveillance, research, tactical planning, and many other evolving applications. Nowadays, the technology is accessible for emergency response on land or moving waters. UAVs can be classified based on altitude, range, endurance, and weight; these vehicles also support a broad scope of utilization, including military and commercial applications [42]. The widespread use of aerial vehicles in different environments introduces the need to implement better deployment and landing stations since many of the most commonly used UAVs, such as the Vertical Take-Off and Landing (VTOL) UAVs, cannot land safely on sloped or rapidly changing surfaces. The vehicle may be unable to maintain flight if it is angled to match an uneven landing surface. This is primarily due to the physics of rotorcraft UAVs, in which the thrust force is perpendicular to the landing gear. [1,16].

Significant work has been done regarding the limitations of ground landing surfaces. Although some research has been done to implement such technology for vehicles to land and deploy on surface water, such as the SpaceX autonomous spaceport drone ship, no commercial system is available on the market. However, designing a dynamic platform to secure UAVs while charging or resting on the sea surface is complex, especially as there are no extant models to emulate. This design project will force the engineer to deal with complex moving parts in a dynamic environment leading to uncertainty. This study concludes that performing motion control in uncertain environments using a mechanism capable of performing pure spherical motion would be a feasible solution for such limitations. The goal of this master's thesis is to explore the application of a spherical parallel manipulator (SPM) in water-surface self-leveling platforms to allow the landing of unmanned vehicles on the surface of dynamic waters.

The unique design of a portable water-surface self-leveling platform for small-scale UAVs is presented in this thesis, with a thorough explanation of how it was implemented and an experimental assessment of its performance. The self-leveling platform under study is designed and tested utilizing open-source and commercially available parts, and parts made in-house. In contrast to other landing platforms, the basic design of this vehicle enhances its utility and versatility while accommodating several commercially available small-scale rotorcraft UAVs.

Chapter 2

2. **Literature Review**

The Research on conventional and aquatic self-leveling devices is examined in this section. The landing platform described in this study is contrasted with earlier work from the University of Denver Unmanned System Research Institute (DU2SRI).

2.1 Self-Leveling Systems

2.1.1 Argo J5

This is a custom-built self-leveling Unmanned Ground Vehicle UGV landing platform attached to the top of the commercially available Argo J5 UGV [2]; refer to Fig.2.1.1-1. This device was built to prevent and overcome challenges that hinder the broad utilization of small-scale quadrotors, helicopters, and fixed-wing UAVs. Said challenges negatively affect these vehicles' endurance, range, and payload to diverse applications. This new landing platform "allows quadrotors/helicopters to take off, land, and possibly recharge while the overall UGV-landing platform system is either stationary or moving" [2].

The platform leveling system must function in challenging terrain (off-road) up to 25° off level and level to within 1° of horizontal [3][4][5][6].

A navigation controller, platform leveling controllers, and accurate dynamic models must be developed for the system to function as an improved ground robotic vehicle. Furthermore, the base UGV vehicle must be stationary or moving for the takeoff and landing to be functional. The moveable landing platform accommodates self-leveling angles up to 25°. The study in [7] places particular emphasis on the connection between design cost and practicality. [8] goes over the construction of high torque platforms and how much weight they can support. Work on a self-leveling system with two degrees of freedom is done in [9]. The self-leveling landing platform and the UGV base vehicle are designed as a single system in [10] and [11], resulting in a cohesive ensemble. In this study, the landing platform of Fig. 2.1.1-1 is subjected to the Euler-Lagrange technique to examine and assess how to level the system quickly [12].

Figure 2.1.1-1: Argo J5 with the custom-built landing platform [12].

2.1.2 Stabilizing Surface for Flight Deck

Another system is a self-leveling landing surface designed to allow helicopters or other vehicles, including fixed-wing unmanned aerial vehicles and rotary-wings vertical take-off UAVs, to land on ships traveling in rough seas [13].In bad weather, operating a helicopter from the deck of a boat is usually impossible, and there have been numerous cases of accidents involving helicopters trying to land on ships that were swaying because of rough seas [14, 15]. A landing surface describes the system mounted on four stacks of rotating columns with inclined mating surfaces. The platform is built to respond quickly to even the slightest shift in the boar's inclination and orientation, although it is not able to correct for angles larger than 15 degrees. [16]

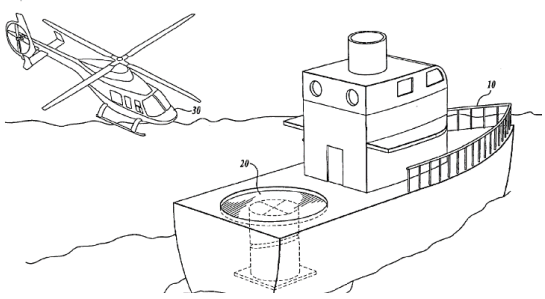

Figure 2.1.1-2: illustrates the flight deck stabilizing system operating on the water's surface [16].

2.1.3 Self-Stabilizing Boat's Deck

This boat operates as an Olympic hurdler where the legs fly up and down to clear obstacles while the frame and head stay leveled even in rough waters. Every corner of the body acts independently as the system is capable of handling motion in 3 degrees of freedom: pitch, roll, and heave. Though people and cargo move around the boat, it remains level due to the changing in the pressure of airbags distributed throughout the body of the boat. Like a pontoon, the vehicle sits on two long hulls shaped like skis connected to a platform at the front and back of the boat through metal arms. The system uses an accelerometer in each corner where the arm meets the hull in order to detect and match the movement of the ocean and uses motors that turn a ball screw that pushes or pulls the control arm lowering and raising that end of the hull as necessary to match the movement of the waves. [17]

2.1.4 Bugatti Self-Leveling Pool Table

Bugatti's branded pool table is made of titanium and a machined aluminum frame covered in carbon fiber. Although having a solid frame, the table fulfills professional tournament requirements and includes many high-end attachments. IXO equipped the pool table with a gyroscopic sensor connected to servo motors in each leg, that can alter table height every five milliseconds to counteract the ocean motion and maintain a level playing surface making the table useable at sea [18]. The pool table is kept level regardless of movements at sea. The platform

automatically changes its position in response to data collected by the sensors. Thanks to this system, it is possible to play while navigating the open ocean. [19]

2.1.5 Autonomous Spaceport Drone Ship

Described in [20] is the autonomous spaceport drone ship (ASDS) designed by SpaceX. Rockets can be launched into space and returned to Earth using technology. To allow recovery at sea for missions that lack the fuel to return to their launch location. The spaceport consists of a massive landing platform that is autonomously operated when on station for a landing, an ocean-going vessel that is often derived from a deck barge with station field engineers. The ASDS is brought to its oceanic position by the spaceport system using a tug signal, and it then follows the landing. To carry the rocket safely to the port, engineers will board the landing platform and secure the rocket. The drone ships will soon be able to receive instructions from an automated identification system (AIS) tracker, aiding in tracking their journey during recovery operations, in place of needing a tug.

Figure 2.1.5-1: SpaceX autonomous drone ship

2.1.6 Other Related Systems

There are several self-leveling systems available in the market today, such as the durable self-leveling platform used on a point-absorbing wave energy conversion buoy [26]. The platform is designed in a manner that it should be able to level itself through its entire expected lifespan. The platform can be used with the winch-drum and transmission chain designs available in the market. It can withstand the challenging conditions encountered when operating at sea. Another similar system would be the ball balancing PID system which focuses on using applied control to build a mechanism that compensates for disturbances and external actions imposed on the system when it is found inherently unstable or semi-stable. It is a ball balancing system with 2 degrees of freedom responsible for controlling the tilt of the plate. The table can be positioned at a specific degree of inclination to offset the motions of the ball thanks to two servo motors.[41]

2.2 Previous Work Within the DU2SRI Group:

This project intends to design a self-leveling platform to overcome limitations and extend the technology used in previous projects within the DU2SRI group. The ISLANDS platform [21, 22] is a sizable, fixed device that may be transported from one place to another on a truck. Next, we have a semi-autonomous mobile self-leveling landing platform for small-scale UAVs that is intended to launch, recover, and re-launch VTOL UAVs without the aid of people. The landing platform is robust, portable, and reasonably priced, making it perfect for civilian applications needing a base station from which a rotorcraft UAV can take off and land in inhospitable terrain. With its sizable onboard lithium batteries and wireless connection, this landing platform can function autonomously for extended durations in isolated regions and self-level on uneven ground and slightly inclined slopes. This thesis analyzes the distinctive design features that distinguish this landing platform from comparable systems, describes the prototype vehicle, and presents experimental findings to prove that the system is fully operational and satisfies all fundamental design requirements [16].

Though both platforms detailed above are developed with the same purpose in mind as the one presented in this thesis, to serve as a fully integrated station for UAV operations in remote locations. They are dedicated to ground operations only. The new landing platform design has solved this limitation by enabling it to level on the surface of the water.

Chapter 3

Concept Selection

This section outlines the concepts considered when designing the manipulator systems and subsystems, consisting of a brief description of the benefits and challenges of implementing each concept.

Motion control is an essential field of automation that deals with the movement of individual parts of a machine in a controlled manner. Machines performing complex motions in an uncertain environment require precise control and actuation. Control deals with the automation and operation of dynamic systems. One can think of a dynamic system as an object excited by external inputs and producing an output. In this study, the input would be the movement of the waves, and the output would be the platform's response reacting to the environmental change. Therefore, studies of different mechanisms and manipulators were carried out to deal with motion on the surface of the water.

3.1 The Stewart Platform

The Stewart Platform is a parallel manipulator made up of a closed-loop chain. This manipulator guarantees motion in 6 axes due to the high sensitivity of the linear actuators, gyroscope, and three-axis accelerometer. Using such a mechanism for a system performing motion control on the surface of the water would be of great advantage as it would guarantee six parameters or six different ways that the body can move, allowing translation and rotation. [43] claims that an airplane is an excellent illustration of a system with six degrees of freedom since it can freely move in three dimensions using its two horizontal axes, X and Z, and its vertical axis, Y. If it has to face up or down, it must pitch, or change the nose's orientation from horizontal X to Y. The plane can use its rudder to modify the yaw such that the wings remain horizontal, and the nose begins to point toward the Z axis if it needs to turn from the X to the Z axis without changing the orientation of its body. Last but not least, because it is frequently believed that the plane's nose is always pointed in the direction of X, moving the aircraft from X to Y will cause it to roll, hence the phrase. The pilot can then perform moves by combining any of these movement characteristics.

The Stewart platform is commonly used to implement systems such as flight simulations, machine tool technology, crane technology, mechanical bulls, and precision platform positionings such as telescopes, antennas, and orthopedic surgery [23]. However, as mentioned above, the systems use linear actuators, which can both be heavy and slow when electrical. Since this thesis research aims

to explore motion control on the surface of the water where a change in angle and inclination to the platform can happen abruptly, electrical actuators would not be the best fit based on physical tests carried out on this concept selection stage. As this project focuses on implementing motion control on the surface of the water, it would not be wise to deal with hydraulic cylinders.

Figure 3.1-1: This figure illustrates a traditional design of the Stewart platform [23].

3.2 Pan and Tilt

A pan-tilt camera system is used in many fields since it can cover more ground than a single fixed camera arrangement. Despite this, many studies rely on platforms that have been factory produced and calibrated and assume that rotation is perfect when the rotation axes line up precisely with the optical axis of the camera. The kinematic configurations, however, may be erroneous or unknown in a user-created setup when a pan-tilting mechanism is arbitrarily put together, invalidating optimal rotation. The model's differences from the actual physics lead to incorrect servo manipulation of the pan-tilting system. Pan and tilt refer to the horizontal and vertical motion, respectively. The pan and tilt system\ is commonly used to mount a camera and move it along the vertical and horizontal plane. The system is generally controlled by a microcontroller unit or Low digital signal processor chip available in the market. A pan and tilt-like platform consist of two motors, each rotating in pan and tilt direction, and these degrees of rotation hypothetically grant the system 360 degrees field of view. Such a system benefits computer vision applications, video surveillance, human-computer interaction, and augmented mixed reality. [24]

To test this concept, two servo motors are mounted in a pan and tilt assembly using an Inertial Measurement Unit (IMU) attached to the top of the breadboard, which is then attached to the pan and tilt configuration. The system is then tested and evaluated based on its reaction time (speed) and the number of ways the body can move. However, It was observed that this configuration would not provide enough and the appropriate degrees of freedom necessary to operate the platform in dynamic waters.

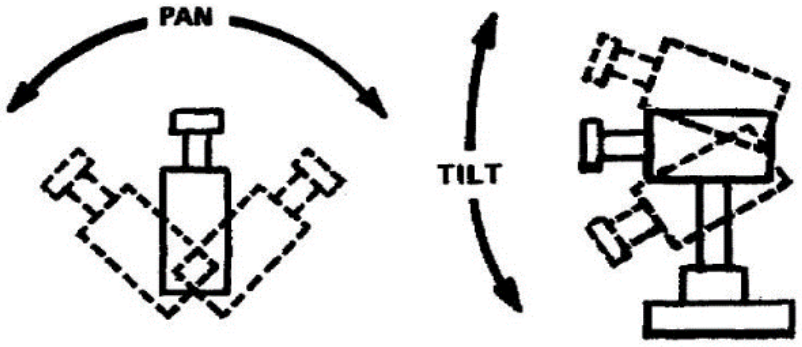

Figure 3.2-1: The figure above illustrates the available degrees of freedom of a traditional pan and tilt system [38].

3.3 Gimbal

A gimbal is a pivoting support that enables item rotation around an axis. An object put on the innermost gimbal may be kept independent of the rotation of its support by using a system of three gimbals, each mounted on the other with orthogonal pivot axes. For instance, despite the ship's pitching and rolling, gyroscopes, shipboard compasses, and shipboard equipment often use gimbals to maintain them upright about the horizon [25]. It is a device most known for its use in the suspension of a compass, according to Philo Byzantium, who wrote about it in the first century of the third century BC [40]. However, the mechanism is employed in much more intricate applications, such as aeronautics, where gimbaled thrust can provide torque vectoring for rocket propulsion [39]. A gimbal would be employed for this research because of its capacity to hold several degrees of freedom and smooth control. The idea is abandoned, nevertheless, because it would necessitate the creation of a gimbal from scratch [26].

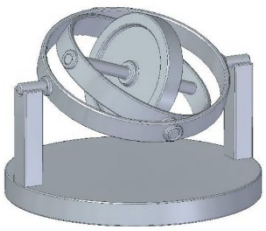

Figure 3.3-1: The figure above illustrates the available degrees of freedom of a traditional gimbal [26]

3.4 Spherical Parallel Manipulators

Parallel manipulators are made up of a mobile platform that is joined to a stationary base by a number of kinematic chains, which are also known as arms [27]. Figure 3.4-1 depicts the fundamental use of this idea. Three arms are connected to the base body, which is at the bottom. Around the vertical axis of the structure, each arm can freely rotate. The mobile platform is connected to the arms by three rigid bodies known as links. Each link is referred to as a binary link since it contains two nodes—one at each end. The nodes serve as attachment places where joints allow for the connection of additional links. This type of system, which consists of a closed-loop chain, enables all the links to move spherically around a single fixed point. A mechanism's degree of freedom is the total number of independent variables needed to identify its spatial configuration fully. Additionally, this number may be calculated as

$$n_{dof} = \lambda\,(n - 1) - \sum_{i=1}^{k} (\lambda - f_i)$$

Where n is the number of links, k is the number of joints, f is the number of degrees of freedom of the ith joint, and lambda is 3 for the planar mechanism and 6 for spatial mechanisms. This system also allows for 3 degrees of freedom which guarantees that the system will be free or move in roll, pitch, and yaw like an airplane. [28]

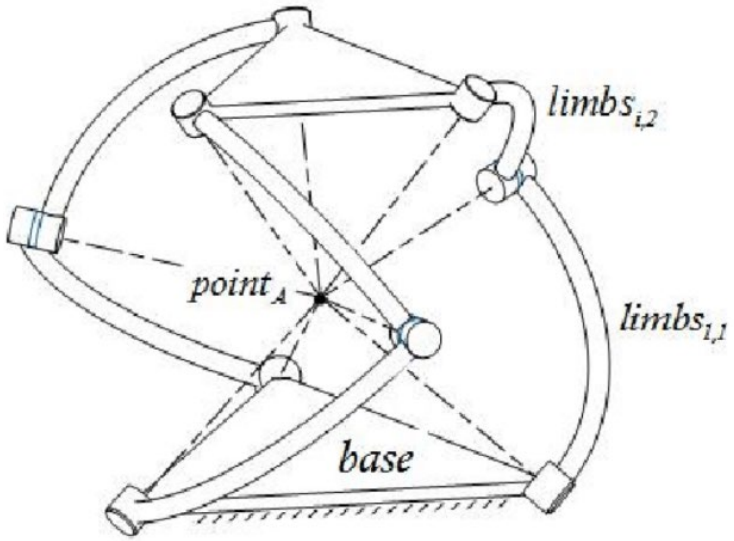

Figure 3.4-1: The image above illustrates the 3-DOF Spherical parallel manipulator [27].

3.5 Design Process

While thinking about implementing the best manipulator system, one of the most important things to consider is the system's degree of freedom, which allows better control precision and symmetry, providing mechanical simplicity and making parts easy to manufacture. With 3 degrees of freedom, the platform can move and autocorrect in yaw, pitch, and roll directions, just like a plane with an angle tolerance of more than 60 degrees. A simple mechanical design, in this case, a symmetric system, decreases any chance of deformation and cracks of parts and minimizes processing, manufacturing, and assembly difficulty. The cost was also a detrimental aspect of the system as most of the parts were fabricated in-house, and one of the targets explored the importance of reducing price without sacrificing the system's quality.

The spherical parallel manipulator was the best choice for this design because it allows for easy implementation and accommodates both critical aspects required for the water-surface self-leveling platform. The table below summarizes the key elements that contributed to the decision of the best concept selection.

Table 3.5-1: Concept selection decision matrix.

	Spherical manipulator	Stewart platform	Pan and tilt	Gimbal
Cost	High	Low	High	Medium
Manufacturing	Medium	Medium	High	Medium
Mechanical Complexity	Low	Low	High	Low
Degrees of freedom	High	High	Low	High

Note: A high score in the Cost area means it cost less

When considering the materials for manufacturing the spherical parallel manipulator, one of the main concerns was the weight of the material. It is beneficial to have the weight be as low as possible. Even Though aluminum is the best choice for the system, 3D printed parts from ABS were used, and most of the crucial parts of the design, such as the link arms, were impossible to manufacture in-house.

Table 3.5-2: Material selection decision matrix

	Aluminum	Carbon Fiber	**ABS**
Cost	High	Low	High
Manufacturing	Medium	Medium	High
Strength	High	High	Low
Weight	Medium	High	High

Various actuator systems were considered during the preliminary design stage. Due to its consistent output and simple manipulation, the DC motor was

considered. While specific DC motors have a maximum torque at low speeds, their torque is constant throughout the speed range, making them best suited for continuous use. A vital component of the system in this study is the ability to control the position of a robot, which is often impossible with a DC motor. Stepper motors, on the other hand, may exert more force from rest and can produce their maximum torque at low speeds, making them extremely helpful in high precision, demanding applications like robotics, 3D printers, and similar systems where position control is crucial [34]. Servo motors have fewer poles than stepper motors, which means they move progressively with a continuous pulse in a closed loop system. However, servo motors need an encoder to alter pulses for position control [35].

Table 3.5.3*:* Actuators decision matrix

	Thrust	Power Consumption	Weight	Control precision	Durability
DC motors	High	Medium	Medium	Low	High
Servo motors	Medium	High	High	Low	Medium
Stepper motors	High	Medium	Medium	High	High

To begin the prototyping and testing phase of the project, a decision had to be made regarding the best microprocessor and a position control sensor that would best fit the project's purpose. The Raspberry Pi 4 (RPI) was chosen as the main microcontroller because it is based on more modern electronics than the Arduino. Further into the design project, it was observed that the RPI would generate considerable delays in PWM signals required for the motor control. Thus,

to mitigate this limitation, a decision was made to use the Teensy child board to operate as a bridge from the RPI to handle the PWM signals better. The Bno055 9-axis absolute orientation sensor was selected over various others due to lower latency during operations and the multiple-axis control.

Table 3.6-4: Main microcontroller decision matrix

Rating -1 to +1	Micro-Controllers			IMU Sensor	
N/A	Arduino	**Teensy**	**Raspberry Pi 4**	9DoF Razor IMU	**Adafruit BNO055**
Price	High	High	Medium	Medium	Low
Operating system	Low	Low	Medium	N/A	N/A
Open source	High	High	High	High	Medium
Power consumption	Low	Medium	High	Medium	Medium
Real-time operation	Medium	Medium	Low	Medium	High
Programming	Medium	Medium	High	Medium	Medium
PWM	Medium	High	Medium	N/A	N/A

Chapter 4

Water-Surface Self-Leveling Landing Platform

The systems studied in this research project features a combination of a traditional three-wheel design with an inventive self-leveling design. The requirements of this platform are its maneuverability and ability to maintain itself leveled on the surface of the water. The prototype is equipped with a high-speed IMU sensor and installed on the actuator to help develop and test real-time maneuvering of the links and base in different scenarios. Based on different dynamics and kinematic architectures, Spherical parallel robots (SPRs) can be defined as 2-DOF SPRs and 3-DOF SPRs. Two serial 3R legs in 2-DOF SPRS connect the end-effector to the base. The common revolute joint found at the end of each leg is then used to bring the two legs together at a common point. The global coordinate system R's origin is where all revolute joint axes intersect [29].

4.1 3-RRR Spherical Parallel Manipulator

The 3-RRR Spherical Parallel Manipulator, a symmetrical 3-DOF mechanism made up of three similar kinematic chains, is the subject of this research project. Three revolute joints, a proximal and a distal link, make up each kinematic chain. Actuators power the proximal links, while passive revolute joints bind the distal links to the moving platform. Fig. shows the 3-RRR manipulator's structural layout. 3. In this part of the book, the most crucial aspects of this robot's kinematic properties are discussed [30].

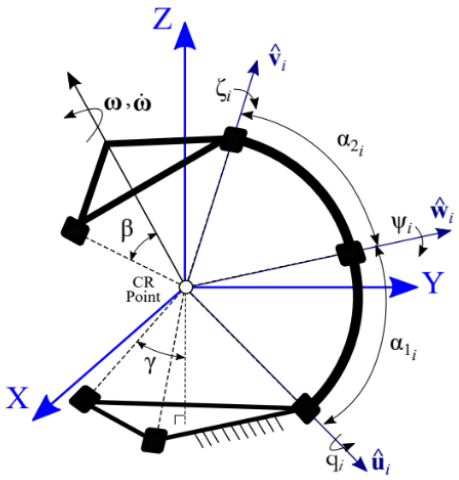

Figure 4.1-1: Schematic, reference, and rotations of a typical spherical parallel manipulator [30].

A spherical equivalent kinematic model was developed. As mentioned above, the model is a parallel mechanism consisting of three identical serial links that are the equivalent of the stepper motors, which we will call manipulators. Each manipulator presents 3 degrees of freedom (DOF) with intersecting axes at the

sphere's center. The equivalent mechanism is created by assigning a serial link manipulator to each stepper and a DOF for each DOF present in the Shaft or sphere interface: roll, pitch, yaw. Using Figure 4.1-1, these DOFs correspond to rotations about X_1, Y_1, and Z_1, respectively. Only one joint is actuated, representing the actuated axis of the stepper motor shaft, and roll about X_1. The other two joints are free, corresponding to the two axes that the sphere spins freely on the motor shaft. Each of these manipulators is interconnected at the center of the sphere, contributing to a common goal.

4.2 Dynamic Model Description

The development of mathematical models that describe the dynamic operation of a system is an essential first step in the automation approach. ZYX fixed-body Euler angles are used to define the orientation of the moving platform for the kinematic analysis of the spherical parallel manipulator. Therefore, the task space variables are defined as $\theta = [\theta_1, \theta_2, \theta_3]^T$. Consequently, the moving platform's rotational matrix can be calculated as

$$R_P^0 = R_z(\theta_1)R_y(\theta_2)R_x(\theta_3) \qquad (1)$$

Which can then be rewritten as

$$R^{06} = \left(R_z^{01}R_y^{12}\right)\left(R_x^{23}R_y^{34}R_z^{45}\right)\left(\left(R_y^{12}\right)^T(R_z^{01})^T\right) \qquad (2)$$

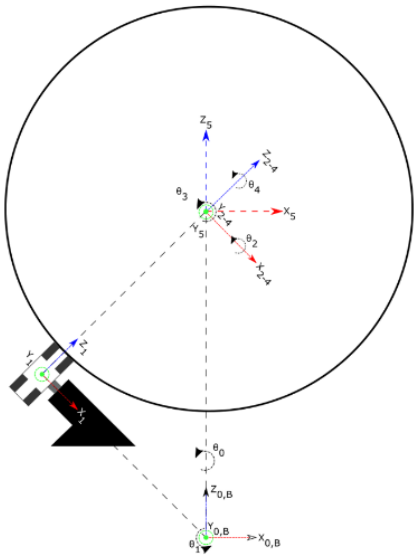

Figure 4.1.2: Reference frames and rotations of one serial manipulator [37].

Where R is the rotation matrix from one frame to another in a moving coordinate frame sequence. Figure 4.1-2 shows the respective XYZ reference frames. For example, is the rotation from frame 0 to 1 about axis Z_0 and is the rotation from frame 1 to 2 of about axis Y_1, etc. [31]. The matrices in Eq. 1 are grouped by parentheses to simplify the discussion. The first group $\left(R_z^{01}R_y^{12}\right)$represents the rotations given by the position of the motor, where is the 45° elevation angle of the motor and is the 120° separation angle between the motors and is therefore constant. The second group, $\left(R_x^{23}R_y^{34}R_z^{45}\right)$ is for the three serial links with intersecting axes, containing rotations representing the degrees of freedom of the actuator's sphere interface. Here is the controllable motor rotation angle, about X_2, and is the free pitch, about Y_3, across the actuators. Less intuitively is the free yaw about Z_4, which represents the twist of the ball that occurs about the sphere's radius, pointing at the tangency between the actuators and the base. The

last group $\left(\left(R_y^{12}\right)^T (R_z^{01})^T\right)$connects the end of the manipulators to the common goal frame. It represents the inverse rotation which returns to base frame coordinates [31,37].

Unit vectors $\hat{u}_i$, $\tilde{v}_i$ and $\hat{w}_i$, for i = 1, 2, and 3, all intersect at the CR point, which is referred to as the origin of the base coordinate system, in the 3-RRR manipulator. Consequently, it is possible to define the unit vector of the primary and intermediate revolute joints as

$$\hat{u}_i = R_z(\lambda_i)R_x(\gamma - \pi)[0,0,1]^T \quad (3)$$

$$\hat{w}_i = R_z(\lambda_i)R_x(\gamma - \pi)R_z(q_i)R_x(\alpha 1_i)[0,0,1]^T \quad (4)$$

Moreover, $\tilde{v}_i$ may be derived as follows:

$$\tilde{v}_i{}^* = R_z\left(\eta_i\right)R_x(-\beta)[0,0,1]^T \quad (5)$$

$$\tilde{v}_i{}^* = R_P^0\, \tilde{v}_i{}^* \quad (6)$$

in which, $\tilde{v}_i{}^*$ represents the unit vector $\tilde{v}_i$ in the initial configuration of the moving platform.

4.3 Inverse Kinematic

A goal rotation is conveniently defined in a Z-Y-X fixed frame.

$$G = R_z(\theta_y)R_y(\theta_p)R_x(\theta_r) \quad (7)$$

The goal parameterization allows for intuitive definition in the standard roll (θ_r), pitch, (θ_p), and yaw (θ_y) angles. The forward kinematic of each arm in Eq. 1 (represented by subscript *i* for each arm: A, B, & C) must equal the same goal:

$$G = R_i^{06} = \left(R_{zi}^{01}R_{yi}^{12}\right)\left(R_{xi}^{23}R_{yi}^{34}R_{zi}^{45}\right)\left(\left(R_{yi}^{12}\right)^T\left(R_{zi}^{01}\right)^T\right) \quad (8)$$

For brevity, the middle group is defined as Mi, and is the only variable group:

$$M_i = \left(R_{xi}^{23}R_{yi}^{34}R_{zi}^{45}\right) \quad (9)$$

G becomes:

$$G = \left(R_{zi}^{01}R_{yi}^{12}\right)M_i\left(\left(R_{yi}^{12}\right)^T\left(R_{zi}^{01}\right)^T\right) \quad (10)$$

Mi represents the 3 DOF serial link manipulator with intersecting axes driven by joint angles, 2 , 3, & 4 , of which only 2 is controllable. Therefore, may be isolated as

$$M_i = \left(\left(R_y^{12}\right)^T\left(R_{zi}^{01}\right)^T\right)G\left(R_{zi}^{01}R_y^{12}\right) \quad (11)$$

Where the subscript *i* is dropped for R_y^{12} and G as these rotations are common for all serial link manipulators. This subscript is also omitted in matrix elements, but these remain the joint angles of the individual manipulator Mi of Eq. 9 can be explicitly written as

$$M_i = \begin{vmatrix} c_3c_4 & -c_3c_4 & s_3 \\ c_2s_3 + s_2s_3c_4 & c_2c_3 - s_2s_3s_4 & -s_2c_3 \\ s_2s_4 - c_2c_4s_3 & s_2c_3 + c_2s_3s_4 & c_2c_3 \end{vmatrix}$$

(12)

Where $s_2 = \sin(\theta_2)$ and $c_4 = \cos(\theta_4)$, etc. For a given goal, the right side of Eq. 11 is entirely known and can be expressed as

$$M_i = \begin{vmatrix} r_{11} & r_{12} & r_{13} \\ r_{21} & r_{22} & r_{23} \\ r_{31} & r_{32} & r_{33} \end{vmatrix}$$

(13)

Where r represents the numerical value of the matrix index. From Eq's. 12 and 13 and omitting irrelevant terms

$$\begin{vmatrix} c_3c_4 & -c_3c_4 & s_3 \\ \ddots & \ddots & -s_2c_3 \\ \ddots & \ddots & c_2c_3 \end{vmatrix} = \begin{vmatrix} r_{11} & r_{12} & r_{13} \\ \ddots & \ddots & r_{23} \\ \ddots & \ddots & r_{33} \end{vmatrix}$$

(14)

The solutions can then be calculated as for an intersecting axes manipulator [21].

$$\theta_{3i} = aTan2\left(\frac{r_{13i}}{\sqrt{{r_{23i}}^2 + {r_{33i}}^2}}\right)$$

$$\theta_{2i} = aTan2\left(\frac{-r_{23i} \times sign(c_{3i})}{r_{33i} \times sign(c_{3i})}\right)$$

$$\theta_{4i} = aTan2\left(\frac{-r_{12i} \times sign(c_{3i})}{r_{11i} \times sign(c_{3i})}\right)$$

(15)

By applying the inverse kinematic equation (Eq. 15) to a target and using the resulting joint angles to determine the mechanism's final frame using the forward kinematic, the inverse kinematic solution is validated as normal (Eq. 8). Error can therefore be roughly described as

$$E_i = G - R_i^{06}(\theta_{2i}, \theta_{3i}, \theta_{4i})$$

(16)

Chapter 5

Mechanical Analysis

The project's primary goal is to achieve motion control of the platform on the surface of the water. When boating, it is crucial to consider the waves' size and direction and whether they are breaking. These factors directly affect by what means the waves impact the platform and how we need to compensate for the steering boat or leveling of the platform. Whether a boat can navigate safely in water depends on the size of the waver it encounters. Compared to someone with a small ship, someone can handle larger waves with a bigger and more powerful boat. To determine the wave height and wavelength conditions, the boat specifications idealized for this research could withstand navigating it safely, and the following rules and formulas were used. According to ocean navigator The Voyager's resource [32], a magazine platform for voyagers who desire to know more about their boats, their gear, and the techniques to make them better voyagers states that “a wave will have enough potential energy to knock your boat down starting at 30 percent of its length”. With that, the formula for calculating the danger wave height for any boat becomes *W Height = B Length x 30%.* By following the rule of 7 or less, which states that if the wave height exceeds the

wavelength at a 1:7 ratio, it may begin to collapse, achieving its breaking point and that allows us to determine the danger wavelength of a boat by using the following formula, *W Length < = W Height x 7 [32]. For instance,* the wave-height danger for a 1-meter (3.37feet) boat starts at 1.001 feet with a danger frequency of 1.44hz. Therefore, anything below these numbers is to be considered a safe navigation condition.

Archimedes' principle states that the buoyancy force is equal to the weight of the displaced water. An object will sink if the weight of the water being displaced is less than that of the object; otherwise, the object will float the boat if the weight of the water displaced and the object is equal. For the purpose of this project, a platform was to be placed on top of a raft so that it could navigate on the surface of the water. This raft was to be circular with 24 inches in width and height. With that, the entire system's volume becomes 2*2*2 = 8. Suppose we define the buoyancy force to be at 0.6, meaning that 505 of the boat sides are out of the water, and by multiplying those two numbers, we get 4.8. Now, if we multiply the current result by the weight of 1 cubic of fresh water 64.2, we obtain 299.51 as the number of ponds of buoyant force that will keep 60 percent of the boat out of the water.

To safely navigate such a mechanism in a body of water, some assumptions must be considered to determine its floating conditions and tipping angle. First, the math is more straightforward, assuming the raft is rigid and has a keel at the bottom. We assume that we will not be navigating in strong wind and waves

conditions, we will not be moving fast, and the platform will be tethered most of the time for testing purposes. Lastly, we assume an ideal scenario in which no water will be inside the raft. Thus, a simple trigonometry analysis was carried out to visualize the typing angle of a platform or boat, considering the characteristics mentioned above.

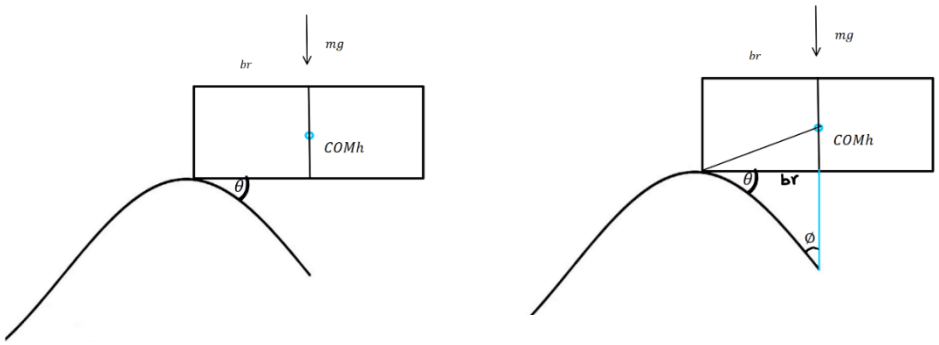

Figure 5-1: Trigonometry analysis to determine the tipping condition of a boat.

With that:

$$mg > \sqrt[x]{(COMh * br)}$$

$$\phi = 90^o - \theta$$

$$\cos\theta\ br < \sin\phi\ COMh$$

The above analysis concludes that the boat or floating mechanism tips over when the right side of the derived equation gets bigger than the left side. Therefore, it is ideal to ensure that the boat geometry against the wave falls on the right side of the equation whenever sealing.

5.1 Structural Analysis

To achieve three degrees of pure rotation, a SolidWorks-designed spherical parallel manipulator platform was assembled from a 3D-printed prototype.

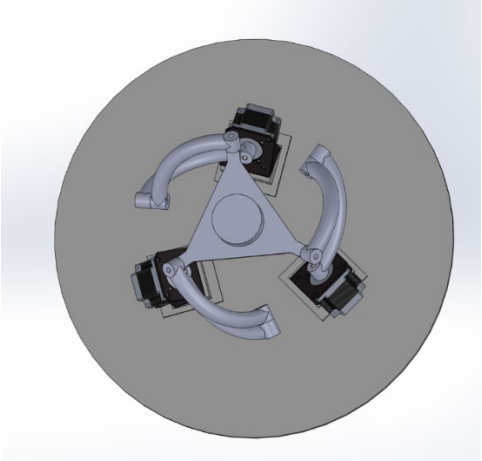

Figure 5.1-1: 3D model of the spherical parallel manipulator platform.

The system should be able to support a weight of at least 5 lbs. on the top platform, but for the following FE analysis, 5 N was applied to the top of each distal link to allow room for further investigation of the material breaking point. Consequently, the experiment demonstrates that the system can handle 5lbs. All stress units are in MPa; for 6063 aluminum, the yield strength is 214 MPa, and for ABS, the yield strength was hard to determine. Based on the following images, we can observe that the deformation and likelihood of the part breaking are more significant when using ABS plastic when a force of 5N is applied to the hole resulting in a max mises stress of +2.681e00. On the other hand, it is safer to use the 6063 Aluminum as it shows less deformation and a mises stress of 3.071e00

when the same amount of force is applied to the link. It is important to note that mises stresses represent the equivalent stress state of the material before the distortional energy reaches its yielding point [33].

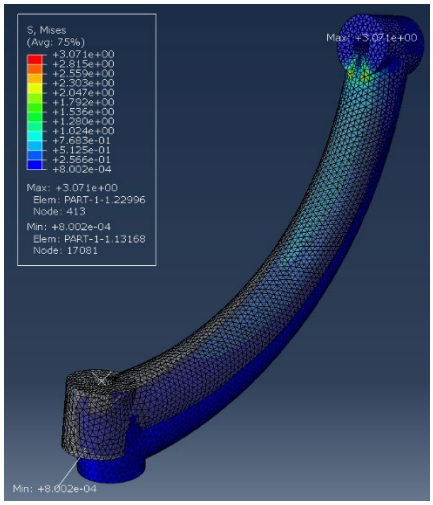

Figure 5.1-2: The image above shows the FE analysis of the 6063 Aluminum when 5N is applied to the link hole safe

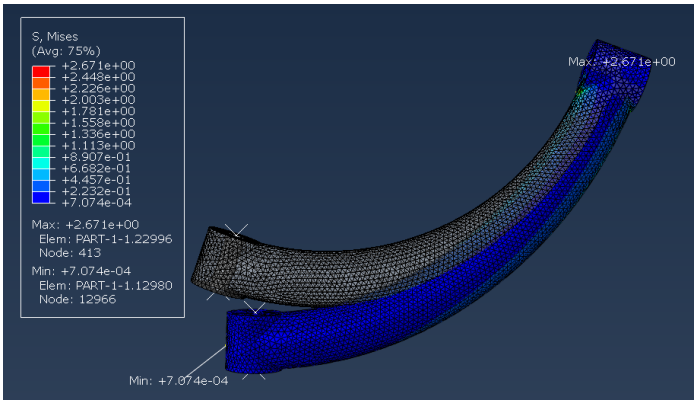

Figure 5.1-3: The image above shows the FE analysis of the ABS plastic link when 5N is applied to the top hole

Chapter 6

Electrical and controls subsystem analysis

6.1 System Block Diagram

The leveling system is broken into subsystems and described in a block diagram, as illustrated in Figure 6.1-1. The main subsystems of the leveling platform, i.e., power and control, are broken down and organized according to physical connections. The power subsystem consists of a Li-ION Power Bank battery that provides power to the microcontroller and motor drivers through a power distribution board to prevent damage from current surges. The control subsystem is divided into two main parts, the ground control station and the onboard system. The ground control station implements of the control strategy used to operate and monitor the leveling platform through a computer connected to VNC. The onboard system includes sensors and motors and contains the functions that send back data to the ground station. The mechanical system included in the diagram consists of proximal and distal links, which significantly affect power consumption and the leveling of the platform.

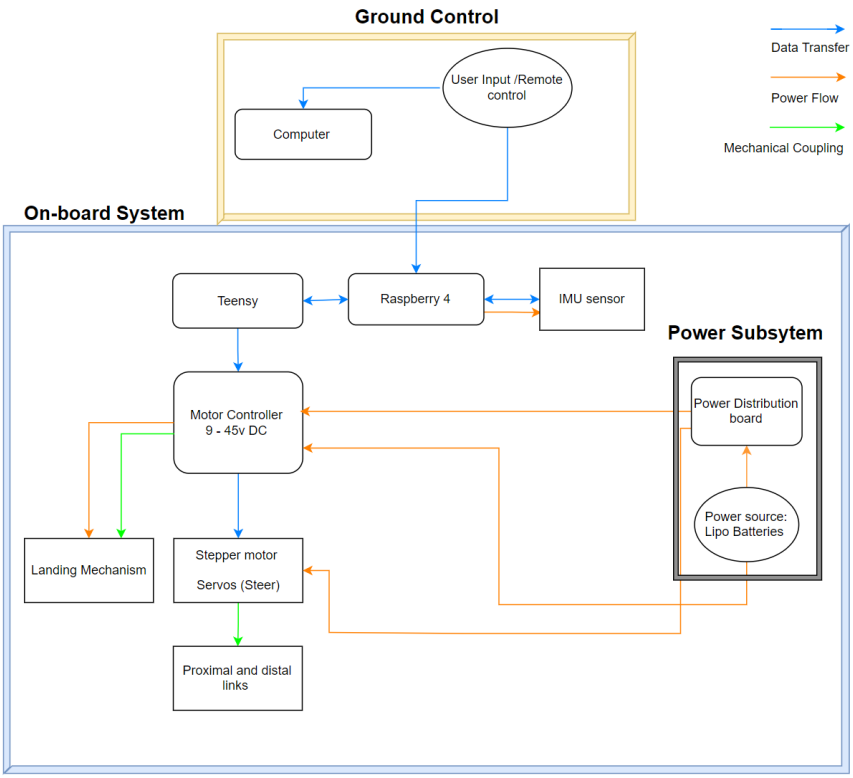

Figure 6.1-1 System block diagram

6.2 Control Subsystem

The control subsystem, shown in Figure 6.2-1, consists of methods and strategies to control and monitor the platform. The onboard system consists of an inertial measurement unit sensor, motors, and microcontrollers, allowing communication with the ground control station. The ground control station allows the user to provide inputs to control the platform using a GUI (Graphical User Interface) connected to the RPI remote connection through VNC. The RPI is the central controller and sends commands to the IMU and teensy, controlling the stepper actuators.

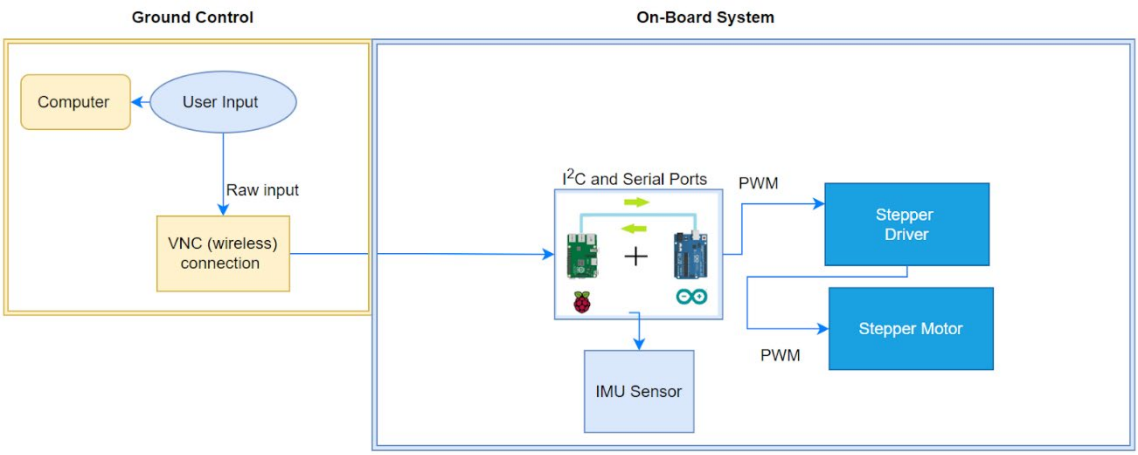

Figure 6.2-1: Control subsystem and communication protocol between devices

6.3 Power Distribution Subsystem

The platform system uses a 12V, 6000mah Li-ION Power Bank battery as its power source. This battery supplies power directly to three motor drivers, providing power to the three stepper motors and using a power distribution board for the RPI and Teensy. During the early stage of the design, individual circuits of each design concept were built and tested, as shown in Figures (6.2-6-) and (6.2-3), respectively. To determine the total run time of the system in full load circumstances, when all motors are running, and with a load on top of the platform, each increasing the torque and current drawn from the battery which raises the need to carry out power analysis calculations. Knowing the motor's stall current and torque limit allows easy analysis and estimate of the current amount of current the system will require from the battery with an estimated max torque of 1.3 N-m,

predicting a battery life of 24 minutes running nonstop. Refer to Tables 6.3-1 presented below for details.

Table 6.3-1: Run time calculations with load - entire system

Load Analysis	Voltage (Volts)	Current (Amps)	Power (Watts)	Run time
Motor Drivers	---	---	---	24 minutes
Stepper Motor	12	12	144	
Microcontroller	5	3	15	
Total	17	15	159	

Battery: 12v, 6AH, 72.0 Wh

Motor Stall current: 20A

Motor Stall torque: 97.2 oz-in = 0.686466 Nm

Derived torque: 1.3Nm

○ Total Runtime = 6AH*6015A = 24 Minutes

Below, the power connections are presented in detail with a schematic of the system. The motor drivers are connected to the teensy board, using 12 digital pins to control the three stepper motors: six are Pulse Width Modulation (PWM) pins, three are digital input/output, and the last pin is for common ground. The battery, RPI Teensy, and motor drivers are attached to the base platform with screws, so they can easily be detached and reinstalled when needed.

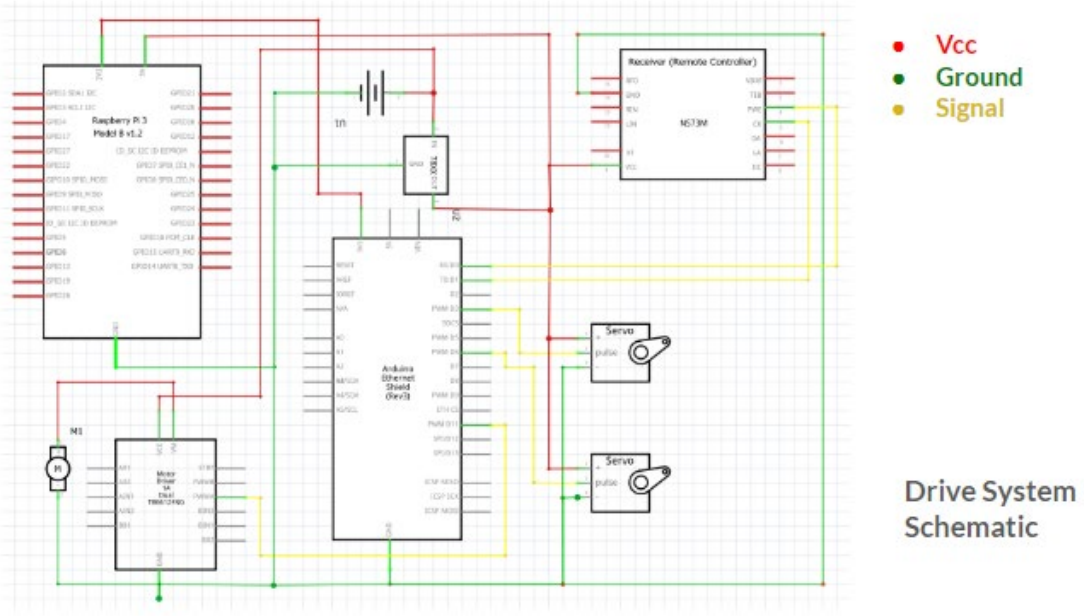

Figure 6.2-2: Schematics for the drive system using the pan and tilt concept.

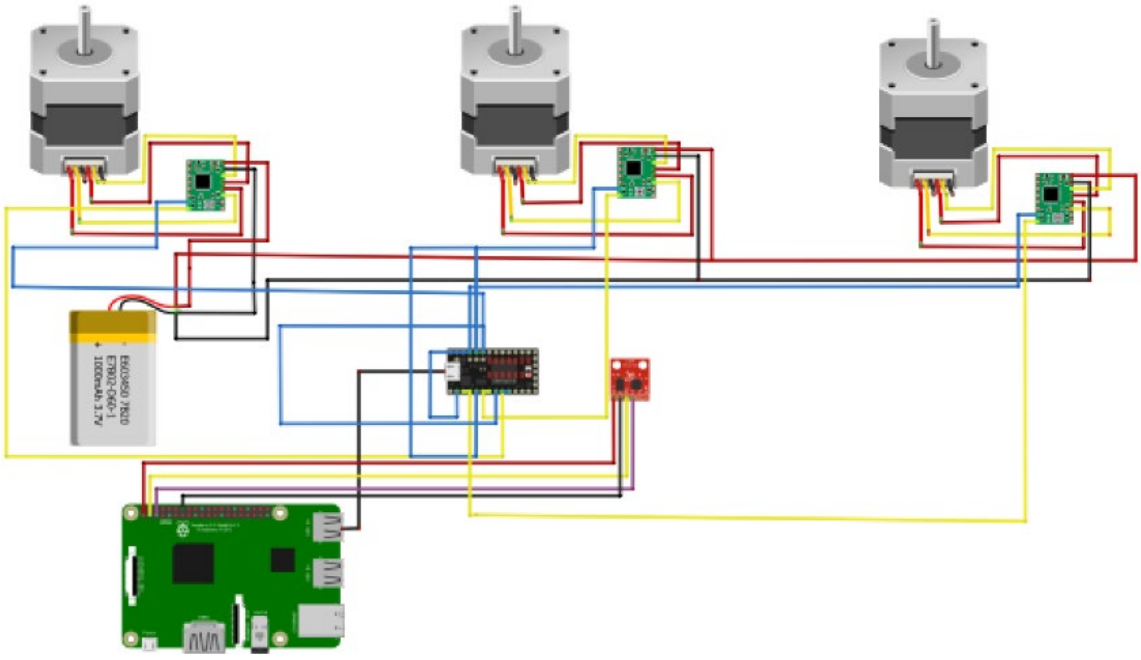

Figure 6.2-3: Electrical diagram for the leveling system

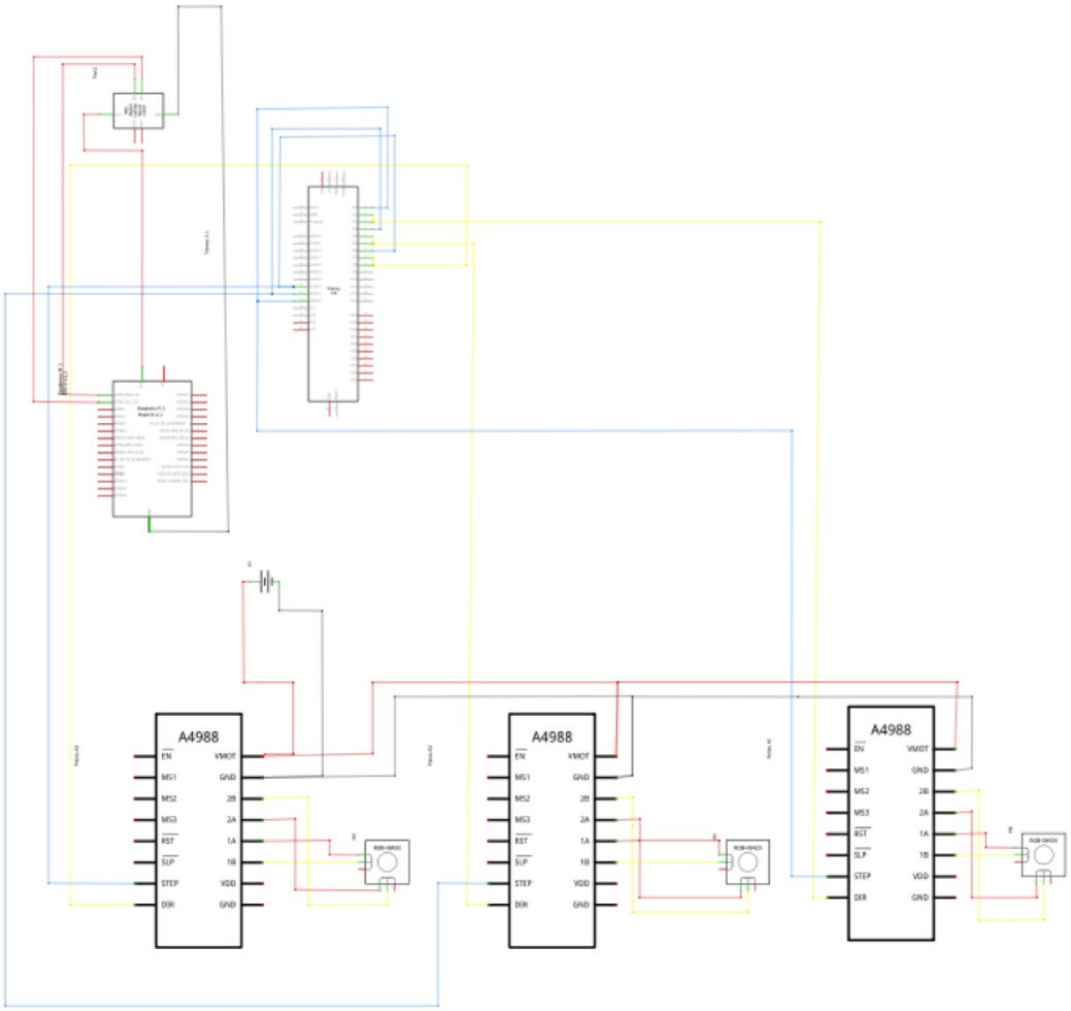

Figure 6.2-4: Schematics for the leveling System.

6.4 Software

In this section, an inertial stabilization, and graphic user interface control system of the SPM prototype is described in detail. Manipulator control for the platform is achieved using a teensy operating as a bridge to a RPI. Manually, the speed of the motors is controlled by the value of the analog PWM wave from the teensy. When sent through the motor driver, this value is converted into steps for the stepper motors. The direction it spins is controlled by the digital signal sent to the direction pin (either - or + value). The platform achieves level by the motors rotating at different velocities and directions when receiving information regarding the sensor's disturbances or changes in inclination. That information is then passed to the PID controller, compensating for angle changes in any direction.

A GUI was created in Python to manually operate the system, in which multiple control functions can be selected. Each function assigns different speeds and directions to the motors and is labeled by how the robot will behave (e.g., clockwise, counterclockwise). These functions can be interrupted by another selected function at any time, making the manipulator responsive. The connection between the RIP and Teensy is possible due to the use of Nanpy, a library that uses Arduino-based boards as a bridge, controlled by a master device like the RPI, where we can run scripts. Nanpy provides powerful libraries, thus making it easy to program.

Wireless communication can be established with the robot, making it possible to control it from anywhere with a computer with internet access, as long as the RPI does. A server (VNC Viewer) is installed on the Pi and can be accessed through a client on a remote computer. The server transmits a duplicate of the Pi's display screen that can be controlled through the client.

6.4.1 PID Controller

PID controllers are frequently used due to their versatility and simplicity. This section details a short PID controller block diagram where the estimation inclination angle of the platform is used as feedback to the PID controller. The RPI microcontroller reads the accelerometer and gyroscope analog signals. The microcontroller will then process this signal after converting it to digital. The inclination of the platform's yaw, pitch, and roll, as well as the angular rate for yaw, will then be determined by combining the digital data. The PID controller will calculate how much to increase and decrease the motor speed and step to keep the platform level whenever it is not at the setpoint.

The proposed PID controller is U(t) - Kp e(t) + Kd e(t)/dt+ Ki e(t)*dt. Where Kp, Kd, and Ki are constant gains, e(t) is the error reading from the IMU sensor, e(t)/dt is the calculated change in error signal over the change in time, and e(t)*dt is the computed change in error over the change in time. That means that the first part of the correction signal is related to the proportional constant, the second part is associated with the derivative of the curve, and the last corresponds to the

integrated area of the curve. During experimental tests, it was observed that having only the proportional controller gain forces the system to overshoot and not autocorrect well. However, when the derivative control is added, the system corrects much quicker, meaning that at some point, the slope of the signal becomes negative, and at that point, the derivative term is not speeding up the signal towards zero; it is backing off by not adding but subtracting from the proportional signal. This allows the platform to slow down and smoothly reach zero, adding to the system's stability. Finally, when the integral control is added to the system, it eliminates the steady-state error that occurs with the proportional controller. In this experiment, Kp, Ki, and kd are tuned manually.

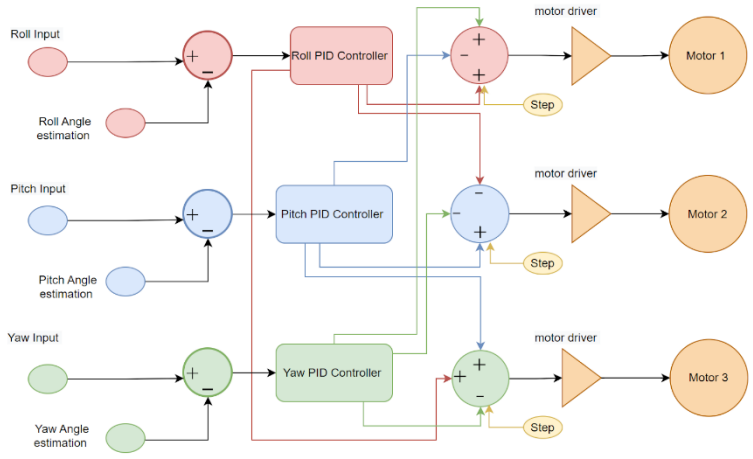

Figure 6.4.1-1: PID controller block diagram, where the intended level angle is the controller's input, while the estimation angle is the controller's feedback. The stepping used to drive the motors is the PID controller's output

Chapter 7

Experimental Results and Discussion

A prototype of the 3 DOF spherical manipulator was assembled with the base and top mobile platform connected by three kinematic chains to validate the approach presented in this research. Three stepper motors actuate the manipulator base joints with a manual PID control algorithm, an IMU is mounted on the manipulator base platform. Actuators and the IMU sensor are connected to the teensy and RPI microcontroller.

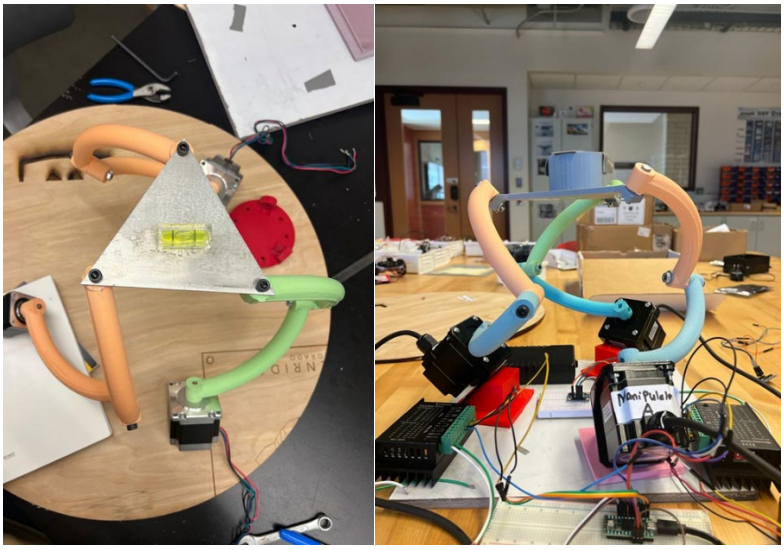

Figures: 7.1 and 7.2 illustrate the initial mechanical and electronic setup of the system

Initial attempts to confirm the inverse kinematic solution as in Eq. 11 were conducted. Results from MATLAB for various goal orientations reveal an error of the order of 1.410-17. Errors in the numerical calculation are the cause of this small numerical disparity.

Different goal orientation trajectories for the platform were extracted from the algorithm. They were stored and extracted as a CSV text file for the roll pitch and yaw of Eq.15. The goal orientation was plotted against the measured reading of the IMU and the error. The trajectory was defined in oscillations between -30° - and 30°. The experimental test in MATLAB was successfully run for two cases: rotations on the roll and pitch orientation. For each rotation pitch and roll, there were 199 set points representing the number of goal orientations evaluated in the experiment.

Refer to figures 7.3 and 7.4 for information on how roll and pitch testing begin with a modest inaccuracy of 1.7 degrees and 0.75 degrees, respectively. Due to the platform's initial configuration, this initial error produces an orientation of infinity for the yaw orientation. This does not, however, account for the quick accumulation of errors, especially in the yaw and pitch directions. Additionally, it was noted that there is a 10° inaccuracy in the measured roll and pitch orientations relative to the goal position orientation. Tests in the yaw orientation failed because the error was too large to analyze the data correctly. It is theorized that the magnetometer in the IMU and probably the fact that the yaw measurement wasn't

calibrated to align with the axis and the offset method are to blame for the recorded figure for yaw drift.

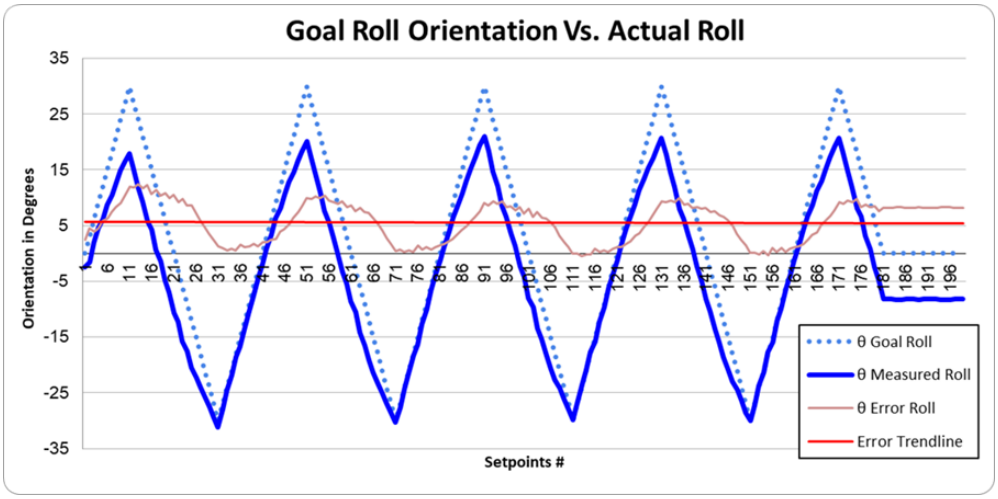

Figure 7.3: The roll orientation plotted against 199 different sets of goal orientation with error measurements.

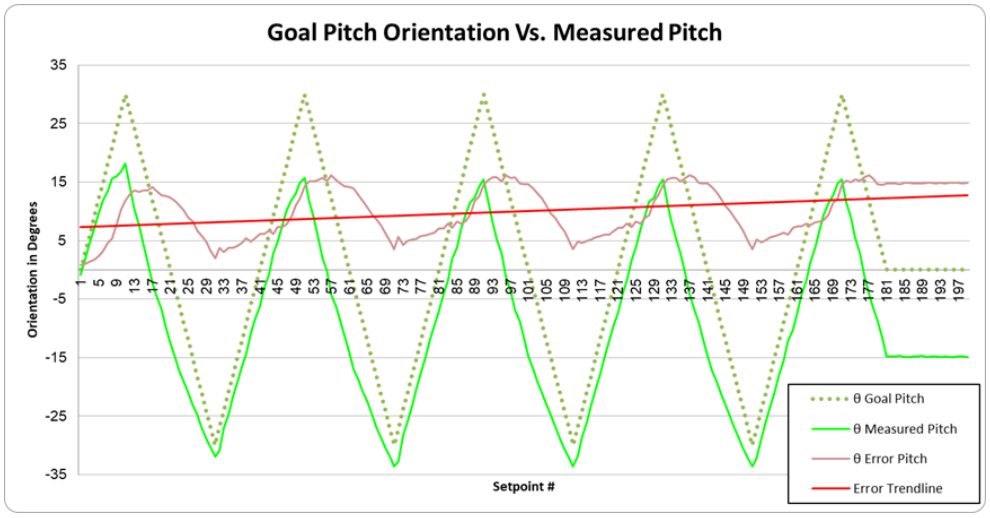

Figure 7.4: The pitch orientation plotted against 199 different sets of goal orientation with error measurements.

Such devices are susceptible to cumulative error due to the magnetometer and gyroscope data fusion, which are significantly impacted by an electrical homogeneous magnetic field (EMF), in this case, EMF emitted by the motor drivers and stepper motors. The IMU, which was used to confirm the alignment of the top platform, is thought to be the source of the cumulative error because it introduces significant measurement errors. Additionally, because the parts may be a little out of tolerance, the 3D-printed components could introduce an error into the total system.

Chapter 8

Conclusion and Future Work

8.1 Future work

The leveling platform prototype is currently still being perfected; however, all the parts are assembled, and the system is undergoing fine-tuning and analysis. Several areas of improvement are being considered throughout this research, such as:

1. Test the platform on the surface of the water.
2. Consider the offset of the IMU from the center of rotation to eliminate the cumulative errors of the system.
3. Determine the time it takes for the IMU to respond when there is a change or disturbance in the system.
4. Filter the PID controller code for better results: All this information coming from the sensor must be accurate to prevent miscalculations that will affect the stability of the leveling of the platform. So, a suitable filter or estimation algorithm is needed to reduce the noise from the sensor to get a near-real value.

5. The PID controller constant gains are tuned manually, contributing to the system's slow response. Therefore, implementing an automatic control would significantly speed up the leveling process.

6. The controller can be combined with other controllers, such as FuzzyLogic. The controller also can be changed using other controllers such as Neural Network. Experimenting with different types of controllers can be an excellent way to compare and choose which one is the best for the application.

8.2 Conclusion

Several issues have been addressed in this research project:

The self-leveling landing platform described in this study is innovative, compact, and designed to extend small VTOL UAVs' water-based autonomy and endurance. The device acts as a base station for aerial vehicles on the water's surface and offers a flat landing platform for unmanned autonomous helicopters and multirotor aircraft. A prototype platform has been manufactured and tested for different scenarios. Initially, the system cannot navigate far-off locations without human assistance or intervention. In some, the self-leveling landing platform described in this study is compact and designed to extend small VTOL UAVs' water-based autonomy and endurance. This concept proves innovative as it improves the range of motion with lower energy requirements resulting in a device that provides low inertia, high velocity, and precise spherical motion.

References

[1]. Doddi, Abhiram. *Vertical Take-off and Landing (VTOL).* University of Colorado, Boulder, CO, 80309, 13 Dec. 2016, https://www.colorado.edu/faculty/kantha/sites/default/files/attached-files/158128-154174_-_abhiram_doddi_-_dec_13_2016_228_pm_-_doddi_report.pdf.

[2]. R. Godzdanker, M. J. Rutherford and K. P. Valavanis, "Islands: a self-leveling landing platform for autonomous miniature uavs", *Advanced Intelligent Mechatronics (AIM) 2011 IEEE/ASME International Conference on*, pp. 170-175, 2011.

[3]. S. A. Conyers, N. I. Vitzilaios, M. J. Rutherford and K. P. Valavanis, "A mobile self-leveling landing platform for vtol uavs", *Robotics and Automation (ICRA) 2015 IEEE International Conference on*, pp. 815-822, 2015.

[4]. M. N. Alghanim, K. P. Valavanis and M. J. Rutherford, "Modeling control and wheel-terrain interaction dynamics of the ugv argo j5", *2019 18th European Control Conference (ECC)*, pp. 1116-1123, 2019.

[5]. M. A. Alghanim, *Modeling and control of the ugv argo j5 with a custom-built landing platform*, 2019.

[6]. M. A. Alghanim, M. Qasim, K. P. Valavanis, M. J. Rutherford and M. Stefanovic, "Comparison of controller performance for ugv-landing platform self-leveling", *Mediterranean Conference on Control and Automation 2020. MED'20*, 2020.

[7].M. J. Zeno and E. GUTIERREZ, “Design of an autonomous self correcting platform using open source hardware,” Faculty of Rensselaer Polytechnic Institute, 2011.

[8].Y. Yu, J. Yi, C. Li, D. Zhao, and J. Zhang, “Control of a rope-driven selfleveling device for leveling adjustment,” in American Control Conference, 2009. ACC’09. IEEE, 2009, pp. 5115–5120.

[9].K. Dalamagkidis, S. Ioannou, K. Valavanis, and E. Stefanakos, “A mobile landing platform for miniature vertical take-off and landing vehicles,” in Control and Automation, 2006. MED’06. 14th Mediterranean Conference on. IEEE, 2006, pp. 1–6.

[10]. R. Godzdanker, M. J. Rutherford, and K. P. Valavanis, “Islands: a selfleveling landing platform for autonomous miniature uavs,” in Advanced Intelligent Mechatronics (AIM), 2011 IEEE/ASME International Conference on. IEEE, 2011, pp. 170–175.

[11].R. Godzdanker, M. J. Rutherford, and K. P. Valavanis, “Improving endurance of autonomous aerial vehicles through intelligent service-station placement,” in Robotics and Automation (ICRA), 2012 IEEE International Conference on. IEEE, 2012, pp. 3179–3184.

[12] Alghanim, Mohammed Aldaoseri, "Modeling and Control of the UGV Argo J5 with a Custom-Built Landing Platform" (2019). *Electronic Theses and Dissertations*. 1638.
https://digitalcommons.du.edu/etd/1638

[13] F. A. Chouery, “Stabilizing surface for flight deck or other uses,” U.S. Patent 7040247 B2, May 9, 2006.

[14] R. Vogelaar. "Black Hawk Helicopter Crashed into a Navy Ship."Internet: http://www.aviationnews.eu/2009/10/23/black-hawk-helicopter-crashed-into-a-navyship/, Oct. 23, 2009 [Feb. 05, 2014].

[15] Los Angeles Times. "Marines Halt Search for Copter Lost at Sea."Internet:http://articles.latimes.com/1998/sep/19/news/mn-24411, Sept. 19, 1998 [Feb. 05, 2014].

[16]. Conyers, Stephen Austin, "A Mobile Self-Leveling Landing Platform for Small-Scale UAVs" (2014). *Electronic Theses and Dissertations*. 789.
https://digitalcommons.du.edu/etd/789.

[17]. VALCARCE, JOSH. “This Self-Stabilizing Boat's Deck Is Always Flat, Even in Rough Waters.” *WIRED*, 29 Oct. 2014, https://www.wired.com/2014/10/velodyne-martini-boat/.

[18]. Gilboy, James. “Bugatti Builds a Self-Leveling Carbon Fiber Pool Table for Its Yacht-Owning Clients.” *The Drive*, 6 May 2021, https://www.thedrive.com/tech/40450/bugatti-builds-a-self-leveling-carbon-fiber-pool-table-for-its-yacht-owning-clients.

[19]. “Pool Table and Boat - Design and Gyroscopic Pool Table by Billards Toulet.” *Billards Toulet EN*, 6 Jan. 2022, https://billard-toulet.us/billiards/pool-table-on-boat/.

[20]. Ackerman, Evan. “SpaceX Planning to Land Autonomous Reusable Rockets on Drone Ships.” *IEEE Spectrum*, IEEE Spectrum, 18 Aug. 2022, https://spectrum.ieee.org/spacex-planning-to-land-autonomous-reusable-rockets-on-drone-ships-next-month.

[21] R. Godzdanker, M. J. Rutherford, and K. P. Valavanis, “ISLANDS: A self-leveling landing platform for autonomous miniature UAVs,” in 2011 IEEE/ASME International Conference on Advanced Intelligent Mechatronics (AIM), pp. 170-175, July 2011.

[22]. R. Godzdanker, M. J. Rutherford, and K. P. Valavanis, “Improving endurance of autonomous aerial vehicles through intelligent service-station placement,” in 2012 IEEE International Conference on Robotics and Automation (ICRA), pp. 3179-3184, May 2012.

[23] “The Basics of the Stewart Platform: Acrome Robotics.” RSS, https://acrome.net/post/the-basics-of-the-stewart-platform.

[24]. Byun, JungHyun Byun, et al. *Accurate Control of a Pan-Tilt System Based on Parameterization of Rotational Motion*. Media System Lab, Department of Computer Science, Yonsei University, Republic of Kore, 1 Dec. 2018, chrome-extension://efaidnbmnnnibpcajpcglclefindmkaj/https://arxiv.org/pdf/1812.00232.pdf.

[25]. Wikipedia contributors. "Gimbal." *Wikipedia, The Free Encyclopedia*. Wikipedia, The Free Encyclopedia, 3 Nov. 2022. Web. 4 Nov. 2022.

[26].Bergman, Anton, et al. “Self-Levelling Platform Concept for a Winch-Based, Single Point Absorbing, Wave Energy Converter.” *KTH Industriell teknik och management*, KTH Industriell Teknik Och Management, 2020, pp. 1–43.

[27]. R. Khezrian, E. Abedloo, M. Farhadmanesh and S. A. A. Moosavian, "Multi criteria design of a spherical 3-DoF parallel manipulator for optimal dynamic performance," *2014 Second RSI/ISM International Conference on Robotics and Mechatronics (ICRoM)*, 2014, pp. 546-551, doi: 10.1109/ICRoM.2014.6990959.

[28]. Soft, Maple. “Position, Orientation and Coordinate Transformations - Maplesoft.” *Maplesoft* https://www.maplesoft.com/content/EngineeringFundamentals/13/MapleDocument_13/Position,%20Orientation%20and%20Coordinate%20Transformations.pdf.

[29]. Wu, Chao & Liu, Xin-Jun & Wang, Liping & Wang, Jinsong. (2010). Optimal Design of Spherical 5R Parallel Manipulators Considering the Motion/Force Transmissibility. Journal of Mechanical Design - J MECH DESIGN. 132. 10.1115/1.4001129.

[30]. Hassani, Ali, et al. Dynamic Models of Spherical Parallel Robots for Model-Based Control Schemes. 1 Oct. 2021, https://arxiv.org/pdf/2110.00491.pdf.

[31]. . J. J. Craig, Introduction to Robotics: Mechanics and Control, 4th ed., USA: Addison-Wesley Longman Publishing Co., Inc., 2018.

[32]. Navigator, Ocean. “Dangerous Waves and Your Boat - Ocean Navigator.” Ocean Navigator 26 Jan. 2022,

https://oceannavigator.com/dangerous-waves-and-your-boat/#:~:text=Remember%2C%20a%20wave%20will%20have,percent%20of%20the%20 boat%20length.

[33]. Kuusisto, Eric. “7 Key Concepts in Understanding Finite Element Analysis.” *LinkedIn*, 8 Feb. 2021, https://www.linkedin.com/pulse/7-key-concepts-understanding-finite-element-analysis-kuusisto-p-e-#:~:text=The%20von%20Mises%20stress%20(%CF%83VM)%20represents%20the%20equivalent%20stress%20state,energy%20(change%20in%20volume).

[34]. Lavaa, Anaa. “The Difference between Stepper Motor and DC Motor.” *Linquip*, 7 June 2022, https://www.linquip.com/blog/difference-between-stepper-motor-and-dc-motor/#:~:text=The%20main%20difference%20is%20that,the%20position%20of%20the%20rotor.

[35]. Motion Control Online Marketing Team. “Servo Motors vs. Stepper Motors in Motion Control: How to Choose the Right One for Your Application.” *Automate*, A3 Association for Advancing Automation, https://www.automate.org/blogs/servo-motors-vs-stepper-motors-in-motion-control-how-to-choose-the-right-one-for-your-application#:~:text=Stepper%20motors%20have%20a%20high,adjust%20pulses%20for%20position%20control.

[36]. Artemiadis , P., Hunt , J. H., & Lee, H. L. (2017, February 3). *A spherical parallel manipulator architecture for shoulder robotic exoskeleton*. Skysong Innovations. Retrieved October 25, 2022, from https://www.skysonginnovations.com/a-spherical-parallel-manipulator-architecture-for-shoulder-robotic-exoskeleton/

[37] Stoianovici, Dan Stephan, "Nyku: A Social Robot for Children With Autism Spectrum Disorders" (2020). *Electronic Theses and Dissertations*. 1843.

https://digitalcommons.du.edu/etd/1843

[38] “The Moving Image and Problem Set.” *Studiomaven*, Arch 200c 2014 Fall, 13 Nov.

2014,

http://studiomaven.org/Course__200c_f14_steinfeld_session_740180.html.

[39] Nasa. (2018). Gimbaled Thrust.

https://www.grc.nasa.gov/www/k12/rocket/gimbaled.html

Offshore Energy. (2018). BOLT Lifesaver runs over 50 days at 100% uptime. https://www.offshore-energy.biz/bolt-lifesaver-runs-over-50-days-at-100-uptime/. (Accessed 2020-04-28)

[40] Sarton, G. (1970). A History of Science. The Norton Library 2. 343-350.

Scientific American. Hollow v. Solid Shafting. 1869. https://doi.org/10.1038/scientificamerican02271869-137b

[41] [2022 Pradeepa S C , Abhijith N, Amoghavarsha S G, Kiran C N, Niranjana Jois H C.

[42] Narayanan, Ram Gopal Lakshmi, and Oliver C. Ibe. “Joint Network for Disaster Relief and Search and Rescue Network Operations.” *Wireless Public Safety Networks 1*, Elsevier, 5 Feb. 2016,

https://www.sciencedirect.com/science/article/pii/B9781785480225500066?vi.

[43] “What Is Six Degrees of Freedom (6DOF)? - Definition from Techopedia.” *Techopedia.com*, Techopedia, 10 Apr. 2019,

https://images.techopedia.com/definition/12702/six-degrees-of-freedom-6dof.